

FlexiWalker: Extensible GPU Framework for Efficient Dynamic Random Walks with Runtime Adaptation

Seongyeon Park
syeonp@snu.ac.kr
Seoul National University
Seoul, South Korea

Jaeyong Song
jaeyong.song@snu.ac.kr
Seoul National University
Seoul, South Korea

Changmin Shin
scm8432@snu.ac.kr
Seoul National University
Seoul, South Korea

Sukjin Kim
iamksj1212@snu.ac.kr
Seoul National University
Seoul, South Korea

Jungkuk Hong
jungkuk16@snu.ac.kr
Seoul National University
Seoul, South Korea

Jinho Lee
leejinho@snu.ac.kr
Seoul National University
Seoul, South Korea

Abstract

Dynamic random walks are fundamental to various graph analysis applications, offering advantages by adapting to evolving graph properties. Their runtime-dependent transition probabilities break down the pre-computation strategy that underpins most existing CPU and GPU static random walk optimizations. This leaves practitioners suffering from suboptimal frameworks and having to write hand-tuned kernels that do not adapt to workload diversity. To handle this issue, we present *FLEXIWALKER*, the first GPU framework that delivers efficient, workload-generic support for dynamic random walks. Our design-space study shows that rejection sampling and reservoir sampling are more suitable than other sampling techniques under massive parallelism. Thus, we devise (i) new high-performance kernels for them that eliminate global reductions, redundant memory accesses, and random-number generation. Given the necessity of choosing the best-fitting sampling strategy at runtime, we adopt (ii) a lightweight first-order cost model that selects the faster kernel per node at runtime. To enhance usability, we introduce (iii) a compile-time component that automatically specializes user-supplied walk logic into optimized building blocks. On various dynamic random walk workloads with real-world graphs, *FLEXIWALKER* outperforms the best published CPU/GPU baselines by geometric means of 73.44× and 5.91×, respectively, while successfully executing workloads that prior systems cannot support. We open-source *FLEXIWALKER* in <https://github.com/AIS-SNU/FlexiWalker>.

CCS Concepts: • Computing methodologies → Parallel algorithms; • Mathematics of computing → Graph algorithms.



This work is licensed under a Creative Commons Attribution-NonCommercial-NoDerivatives 4.0 International License.

EUROSYS '26, Edinburgh, Scotland UK

© 2026 Copyright held by the owner/author(s).

ACM ISBN 979-8-4007-2212-7/26/04

<https://doi.org/10.1145/3767295.3769358>

Keywords: Dynamic Random Walks, GPU Optimization

ACM Reference Format:

Seongyeon Park, Jaeyong Song, Changmin Shin, Sukjin Kim, Junguk Hong, and Jinho Lee. 2026. FlexiWalker: Extensible GPU Framework for Efficient Dynamic Random Walks with Runtime Adaptation. In *21st European Conference on Computer Systems (EUROSYS '26)*, April 27–30, 2026, Edinburgh, Scotland UK. ACM, New York, NY, USA, 16 pages. <https://doi.org/10.1145/3767295.3769358>

1 Introduction

Random walks [6, 8, 10, 12, 36, 39, 42, 58] are pivotal for uncovering structural properties and patterns that drive a broad array of graph-based applications [2, 5, 13–15, 21, 40, 52, 63, 64]. They are particularly effective at distilling core information from large graphs by working on significantly reduced substructures. Among the many variants, *dynamic random walks* [6, 8, 12, 42, 58] have become especially popular because they capture high-order patterns and temporal interactions that static walks miss.

Although numerous graph-processing frameworks exist [11, 24, 30, 46] and span diverse platforms [20, 26, 29, 44, 45, 57], random walks map suboptimally onto them. In contrast to message-passing workloads, a random walk must track a *walker* and repeatedly compute a probability distribution over the current node's neighbors. This fundamental difference demands a distinct set of optimizations.

A variety of CPU- and GPU-based systems address random walks [17, 23, 31, 37, 43, 48, 53, 55, 56, 61, 62], but the vast majority target *static* walks. For static walks, it is profitable to pre-compute and cache per-node transition probabilities—an approach that amortizes the dominant cost of constructing such probability distributions [37, 48, 53].

Unfortunately, such reuse techniques do not extend well to *dynamic* walks. Here, transition probabilities depend on the walker's history and are revealed only at runtime, forcing each instance to regenerate distributions on demand. This regeneration incurs repetitive preprocessing or auxiliary data structure construction costs. Consequently, a framework dedicated to dynamic random walks is needed.

To build such a framework, we first surveyed existing sampling strategies [35, 49–51] used in prior CPU/GPU systems and assessed their relative compatibility for dynamic walks and massive GPU parallelism. Among them, we identify rejection sampling and reservoir sampling as the most practical choices for dynamic walks.

A closer examination reveals optimization opportunities in the state-of-the-art (SOTA) GPU implementation of both sampling methods. The leading rejection sampling design [17] pays a heavy price for global reductions to compute the maximum transition weight—unnecessary work that we eliminate by computing a bound that does not harm the functionality of sampling. The SOTA reservoir sampling kernel [31] suffers from redundant memory traffic and random-number generation. To mitigate these overheads and boost throughput, we adopt an alternative statistical method and a jumping technique for random number generation [9, 16].

However, neither of the optimized kernels is a universal winner. Performance depends on runtime conditions—especially the edge weight distribution, which can shift even within a single walk and can be significantly skewed. We therefore devise a lightweight first-order cost model that selects the faster method *per node at runtime*.

Combining these pieces, we build FLEXIWALKER, a GPU framework that delivers efficient dynamic random walks across diverse workloads. Users write only lightweight workload-specific functions; FLEXI-COMPILER statically analyzes them to generate specialized building blocks, FLEXI-RUNTIME chooses the best sampling strategy on the fly, and FLEXI-KERNEL supplies highly optimized kernels. To the best of our knowledge, FLEXIWALKER is the first framework to explore how the optimal sampling strategy varies per sampling instance during dynamic random walk execution. Such a design is enabled with the tight integration of the compiler component, selection strategy, and kernel optimizations.

We evaluate FLEXIWALKER on five widely used dynamic random walk workloads and compare it with representative CPU and GPU baselines. FLEXIWALKER consistently provides optimized solutions where others cannot and achieves geometric mean speedup of 73.44× and 5.91× over the best-performing CPU and GPU baseline cases, respectively. We release FLEXIWALKER in <https://github.com/AIS-SNU/FlexiWalker> to facilitate its use.

Our contributions can be summarized as follows:

- We analyze GPU sampling techniques for *dynamic* random walks and find rejection and reservoir sampling more suitable compared to other techniques when accounting for runtime dynamics and massive parallelism.
- We optimize both techniques to significantly improve performance by removing global reductions, redundant memory traffic, and random number generation.
- A lightweight first-order cost model selects, at runtime and on a per-node basis, the faster sampling method. The cost

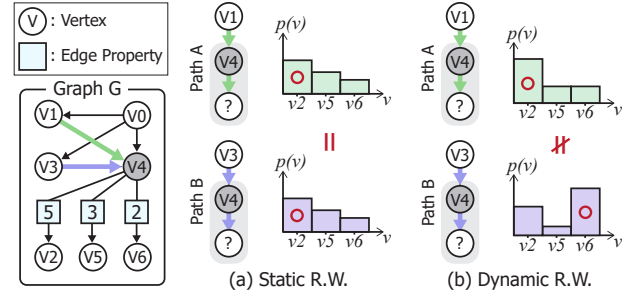


Figure 1. Single step of static and dynamic random walks.

model ensures robust performance under highly skewed and time-varying edge-weight distributions.

- By combining compile-time specialization, adaptive runtime selection, and optimized kernels, FLEXIWALKER requires users to supply only workload-specific logic while automatically delivering state-of-the-art performance.
- FLEXIWALKER surpasses the best-performing cases of CPU and GPU baselines by geometric means of 73.44× and 5.91×, respectively, and successfully runs workloads that prior systems could not support efficiently.

2 Background and Analysis

2.1 Dynamic Random Walks

Let $G = (V, E)$ be a directed graph with node set V and edge set E . For $v \in V$, let $N(v)$ denote the neighbors of v , and let $d(v)$ denote its degree. For $(v, u) \in E$, $h(v, u) \in \mathbb{R}$ denotes the corresponding edge property weight (i.e., intrinsic edge weight in the graph dataset).

In a random walk, a walker repeatedly selects one of its neighbors (referred to as a *step*) until the predetermined walk length is reached. To determine the next node at each step, a probability distribution over the neighbors is required. This distribution is constructed from both property weights h and workload-specific weights w assigned according to the target walk algorithm. The resulting edge transition weight \tilde{w} and the transition probability of moving from node v to u is defined as:

$$\tilde{w}(v, u) = w(v, u) \cdot h(v, u),$$

$$p(u) = \frac{\tilde{w}(v, u)}{\sum_{t \in N(v)} \tilde{w}(v, t)} \quad \text{for } u \in N(v). \quad (1)$$

Unless specified as property or workload-specific, we use the term *weight* to refer to the final transition weight \tilde{w} .

Random walk algorithms are classified as *static random walks* or *dynamic random walks*. If the raw edge property values are used directly to build the distribution, i.e., $w(v, u) = 1$, the process is referred to as a static random walk. In contrast, if the edge property weights are transformed or adjusted to compute new transition weights based on runtime-specific traits, the process is called a dynamic random walk.

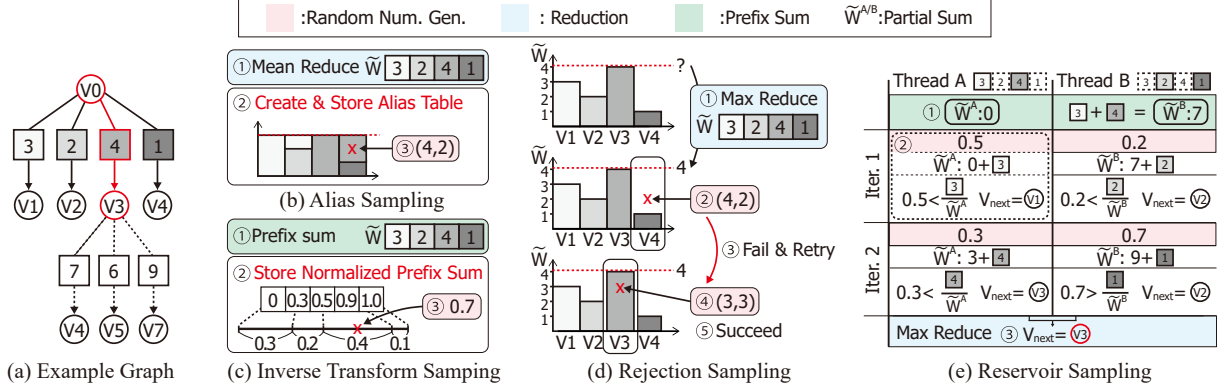


Figure 2. An example of a random walk step and how different sampling methods select the next target node.

Fig. 1a shows a step of a static random walk. The transition probabilities are identical for walkers that moved from v_3 to v_4 and from v_1 to v_4 , indicating that the probabilities remain fixed. However, in the dynamic random walk illustrated in Fig. 1b, the probability distribution for the next step differs even though the current node is the same (v_4) for both paths A and B; the difference arises from their distinct previously visited nodes.

Because the goal of random walks is to extract meaningful node sequences that reflect graph structure and semantics, dynamic random walks are generally more expressive. Representative dynamic walks such as Node2Vec, MetaPath, and Second-Order PageRank incorporate graph topology, user inputs, or task-specific functions into the weighting process.

Node2Vec [12] considers the last visited node and updates the transition probability accordingly. It modifies $h(v, u)$ by multiplying it with tunable parameters a and b . Given the current node v and the previously visited node v' , the workload-specific weight $w(v, u)$ is determined by $\text{dist}(v', u)$, the distance between v' and u :

$$w(v, u) = \begin{cases} \frac{1}{a}, & \text{if } \text{dist}(v', u) = 0, \\ 1, & \text{if } \text{dist}(v', u) = 1, \\ \frac{1}{b}, & \text{if } \text{dist}(v', u) = 2. \end{cases} \quad (2)$$

MetaPath [8] operates on graphs with edge labels. Given an input schema—an ordered set of labels—the walk must follow this schema while traversing the graph. For example, if the schema is (0, 1), the first step must follow an edge labeled 0 and the second step an edge labeled 1. This effectively sets the values of w to 0 or 1 in accordance with the schema.

Second-Order PageRank (2^{nd} PR) [58], like Node2Vec, adjusts neighbor weights based on their connection to the previously visited node and also incorporates the degree of said node. Given $\max_d = \max(d(v), d(v'))$ and a tunable parameter γ , the workload-specific weight $w(v, u)$ is:

$$w(v, u) = \begin{cases} ((1 - \gamma)/d(v) + \gamma/d(v')) \cdot \max_d, & \text{if } \text{dist}(v', u) = 1, \\ ((1 - \gamma)/d(v)) \cdot \max_d, & \text{otherwise.} \end{cases} \quad (3)$$

2.2 Analysis of Sampling Strategies

Random walks incur highly irregular memory accesses, and transforming transition weights into a probability distribution demands non-trivial computation. The procedure for choosing the next neighbor, including this conversion, is referred to as *sampling*. Existing GPU-based implementations [17, 31, 37, 53] typically adopt a specific *base sampling method* (e.g., alias sampling [51], inverse transformation sampling [35], rejection sampling [50], or reservoir sampling [49]) and parallelize it to maximize GPU utilization.

Fig. 2 illustrates four commonly used sampling methods on the example graph in Fig. 2a. In this example, the current node v_0 has four neighbors v_{1-4} with edge weights $\tilde{w}(v_0, \cdot) = \{3, 2, 4, 1\}$, yielding $p(v_0, \cdot) = \{0.3, 0.2, 0.4, 0.1\}$ for a static random walk. Suppose the walker randomly selects v_3 as the next node ($v_0 \rightarrow v_3$).

Figure 2b depicts alias sampling [51] (ALS), used in SKYWALKER [53]. It constructs an auxiliary structure, the alias table, to mitigate random access overhead in weighted sampling. ALS distributes weight values across the table as evenly as possible and stores their positions, allowing the next node to be chosen by generating two random numbers that form a 2D lookup coordinate. Building the table requires a mean reduction over the edge weights, followed by splitting and redistributing blocks that exceed the mean to other indices.

Similarly, inverse transform sampling [35] (ITS) in C-SAW [37] selects the next node with a single random number as shown in Fig. 2c. C-SAW's ITS constructs a cumulative sum distribution by prefix-sum calculation and normalization. Given a random number in (0, 1), ITS requires a binary search to find the node that the random number indexes.

In contrast, the sampling techniques in Fig. 2d and Fig. 2e do not build any auxiliary data structures. Figure 2d shows rejection sampling [50] (RJS), as used in NEXTDOOR [17]. Using repetitive trials with (x, y) 2D random coordinates, a node is accepted only if the y -value falls within its weight range; otherwise, the trial is rejected. Like ALS, RJS needs a reduction to find the maximum weight, but it merely uses it

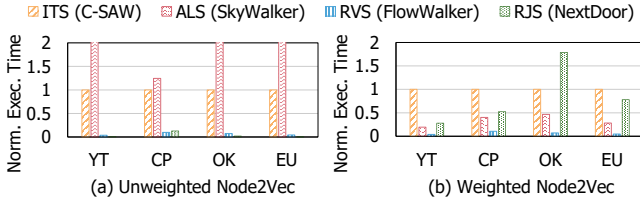


Figure 3. Performance comparison across various sampling methods. Execution time for (a) unweighted Node2Vec and (b) weighted Node2Vec is normalized to ITS (C-SAW).

as the upper bound for generating y instead of constructing a table.

Finally, Fig. 2e illustrates reservoir sampling [49] (RVS), employed by FLOWWALKER [31], the state-of-the-art GPU framework for dynamic walks. RVS visits neighbors sequentially while maintaining a single candidate node: neighbor i replaces the current candidate if $u < \frac{w_i}{\sum_{k=1}^i w_k}$ with $u \sim \text{Uniform}(0, 1)$; otherwise, the candidate is unchanged. FLOWWALKER parallelizes RVS by noting that each comparison is independent once the prefix sums $W_i = \sum_{k=1}^i w_k$ are available, and uses a max reduction to obtain the final target node. Computing the prefix sum and reduction requires inter-thread communication. Although generating one random number per neighbor incurs some cost, the absence of intermediate dependencies allows efficient parallelization on GPUs. For details on the parallelization of RVS, please refer to [31].

3 Kernel Designs for Efficient Dynamic Random Walks

3.1 Performance Comparison on Existing Sampling Methods

Choosing the right sampling method is the critical first step in building an efficient framework for dynamic random walks. We believe RJS and RVS are preferable because they do not have the overhead of repetitive auxiliary data structure construction associated with ALS and ITS. To demonstrate, we measured the runtime of GPU-based random walks that use each sampling method in Fig. 3 on four datasets [3, 4, 27]. We used Node2Vec [12], introduced in Section 2.1, as a representative dynamic random walk workload for comparison.

Figure 3a shows the performance for unweighted Node2Vec, where the edge properties are uniform (i.e., $h = 1$), and Fig. 3b shows the weighted counterpart. As expected, the current baseline implementations of ITS and ALS exhibit significantly longer execution times than the best-performing method, primarily due to the repeated overhead of building auxiliary data structures. This confirms that RJS and RVS are preferable for dynamic random walks. However, we also observe that the optimal sampling method depends on the environment (i.e., traits of the random walk workload). In unweighted Node2Vec (Fig. 3a), NEXTDOOR with RJS overall

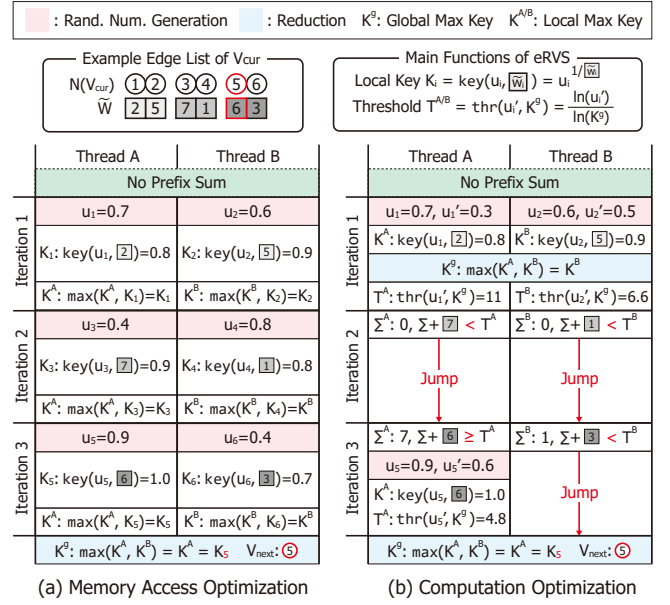


Figure 4. Proposed optimizations of eRVS.

performs the best, whereas in weighted Node2Vec (Fig. 3b), FLOWWALKER with RVS outperforms the others, and RJS runs much more slowly.

These observations led us to select RJS and RVS as the most promising candidates for GPU-based sampling in dynamic random walks. In the remainder of this section, we present novel optimizations for each of these methods, which are the first contributions of this paper.

3.2 Reservoir Sampling Optimization

Despite the advantages of the RVS approach, the current state-of-the-art GPU-based RVS kernel implementation [31] (hereafter called the *baseline RVS kernel*) suffers from two issues: excessive memory access (due to prefix sums) and high computational cost. First, the baseline RVS kernel requires the sum of the preceding edge weights for each neighbor visited. This necessitates full access to the weights and the computation of a prefix sum before sampling. Second, the number of random number generations grows exactly in proportion to the current node's degree, whereas other samplings require far fewer random numbers. To tackle these two bottlenecks simultaneously, we propose eRVS, an enhanced RVS kernel that greatly reduces both memory accesses and random number generations.

To reduce memory accesses, eRVS first eliminates the prefix sum by adopting a statistically equivalent reservoir-sampling method [9, 16]. We illustrate this method in Algorithm 1 and its parallel version in Fig. 4a. Algorithm 1 converts the sampling step into an *argmax* problem by assigning each neighbor i a key $k_i = u_i^{1/w_i}$, where $u_i \sim \text{Uniform}(0, 1)$. After the keys are generated, the neighbor with the globally largest key (k^Q) is selected as the next target of the walk. Intuitively, each key comprises two factors that determine its

Algorithm 1 RVS with Reduced Memory Access

Inputs: v_{cur} : the current walk vertex (target);
 $N(v_{cur})$: the neighbor sequence of v_{cur} ;
 $\tilde{w}_{(\cdot)}^j$: the dynamic weights of $N(v_{cur})$ in walk step j ;

```

1:  $k^g \leftarrow -\infty$ ;  $v_{next} \leftarrow \text{None}$ 
2: for  $i \leftarrow 1$  to  $|N(v_{cur})|$  do
3:    $u_i \leftarrow \text{Uniform}(0, 1)$ 
4:    $k_i \leftarrow u_i^{1/\tilde{w}_i^j}$ 
5:   if  $k_i \geq k^g$  then  $k^g \leftarrow k_i$ ;  $v_{next} \leftarrow v_i$  end if
6: end for
7: return  $v_{next}$ 

```

magnitude: u_i supplies the *randomness* of the walk, and $1/\tilde{w}_i$ acts as a *fixed regulator* of that randomness. This strategy removes the need for a prefix sum over the weights, roughly halving the costly memory accesses to the weights.

eRVS further reduces the computation by cutting the number of random number generations with the *jump* technique [7, 9, 16]. Rather than simulating every event with a random key, we exploit the distribution that governs the number of neighbor evaluations required before a candidate update occurs. By sampling from this distribution once, we can directly “jump” to the neighbor that triggers the update.

According to [9], the update to v_{next} occurs at neighbor s_m for which

$$\sum_{i=1}^{m-1} \tilde{w}_{s_i} < \ln(u)/\ln(k^g) \leq \sum_{i=1}^m \tilde{w}_{s_i}, \quad (4)$$

where $\{s_1, s_2, \dots\}$ is the set of assessed neighbors.

Figure 4b illustrates the overall parallel jump process. To initialize, in the first iteration, each thread first computes a key for one neighbor, as shown in Algorithm 1. The resulting keys are reduced to obtain the initial shared global maximum k^g . With this global maximum in hand, each thread generates a threshold $T = \ln(u)/\ln(k^g)$ and scans its assigned neighbors until the condition in Eq. (4) is satisfied. For example, in thread A’s second iteration in Fig. 4, the local cumulative weight Σ does not satisfy Eq. (4). Therefore, it can skip the random number generation and corresponding key generation—in other words, it jumps this iteration. However, in the third iteration, Eq. (4) is satisfied. Therefore, the thread computes both the key for the current neighbor and a new threshold for the following iterations. This overall process is repeated until all neighbors have been scanned and the local max keys are reduced to obtain the next target node.

3.3 Rejection Sampling Optimization

We propose eRJS, a random walk kernel that uses rejection sampling and greatly reduces the memory access bottleneck of the current baseline rejection sampling method. Typically, the bottleneck of RJS is similar to that of RVS—full access to the entire transition weight list. To minimize the number of retries for each random number generation,

RJS sets the range of the generated random numbers to be $[0, \max(\tilde{w}(v, u))]$ for $u \in N(v)$. For example, in Fig. 2d, the range should be $[0, 4]$. However, this procedure requires a max reduction over all transition weights of the neighbors, which entails full access to the list. Fortunately, an interesting optimization exists. When the maximum transition weight is already known, the max reduction is unnecessary, and sampling involves only iterative random number generation; memory is accessed only for the edge weights selected by the x -dimension of the random number.

Node2Vec [12] in an unweighted setting ($h = 1$) is one such example. If $a = 1$ and $b = 0.5$ in Eq. (2), the maximum is automatically 2 and the range is $[0, 2]$. For other scenarios (e.g., weighted Node2Vec or 2nd PR), however, it is infeasible to precompute the maximum without calculating all edge transition weights.

Instead of obtaining the actual maximum value, eRJS uses a theoretical upper bound computed on the fly. The key insight is that exact knowledge of the maximum edge weight is unnecessary; an upper bound that is equal to or larger than the maximum weight suffices. This allows us to eliminate the max reduction at the cost of potentially more failed sampling attempts caused by additional empty space in the 2D table, while maintaining the functionality of the sampling itself.

We first prove that using an upper bound that is equal to or larger than the maximum weight does not harm the functionality of RJS. In other words, a neighboring node is sampled with the same probability distribution when using the exact max weight and an upper bound larger than said weight. Intuitively, given the i th neighbor’s sample probability $p(v_i)$ and an upper bound c , the relative probability of v_i being sampled over v_j is kept since $\frac{(p(v_i)/c)}{(p(v_j)/c)} = \frac{p(v_i)}{p(v_j)}$.

Next, we provide a more formal proof for using an upper bound by emulating a random walk sampling instance for the target node u . We use \mathcal{N} and \deg instead of $N(u)$ and $d(u)$ for readability. Given the definition of RJS [41], we define the following probability mass functions (PMFs) on \mathcal{N} :

$$\begin{aligned}
p : \mathcal{N} &\rightarrow (0, 1] : \text{target PMF, where } \sum_{v \in \mathcal{N}} p(v) = 1 \\
q : \mathcal{N} &\rightarrow (0, 1] : \text{proposal uniform PMF,} \\
&\quad \text{where } q(v) = 1/\deg \text{ for all } v \in \mathcal{N} \\
c : &\text{any constant such that } c \geq \max_{v \in \mathcal{N}} \frac{p(v)}{q(v)}.
\end{aligned} \quad (5)$$

Using these definitions, the upper bound in eRJS is $\frac{c}{\deg}$, since $p(v) \leq cq(v) = \frac{c}{\deg}$. Moreover, the definition of c guarantees that $\frac{p(v)}{cq(v)} \leq 1$ holds for every v . Note that we chose a uniform PMF for q to simulate the implementation of RJS.

Using the above, we represent a random walk step as:

1. *Propose X*: Draw $X \sim q$ (i.e., uniformly from \mathcal{N})
2. *Draw U*: Draw $U \sim \text{Uniform}(0, 1)$
3. *Accept/Reject*: *Accept* if $U \leq \frac{p(X)}{cq(X)} = \frac{p(X) \cdot \deg}{c} (\leq 1)$. Otherwise *reject* and return to 1. The accepted value is the *sample*.

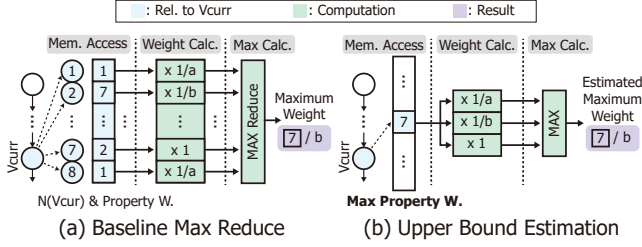


Figure 5. Optimizing rejection sampling with eRJS.

We can now define the probability of accepting a certain node v :

$$\begin{aligned} \Pr[\text{sample} = v] &= \Pr[X = v \ \& \ \text{accept}] \\ &= \Pr[X = v] \cdot \Pr[U \leq \frac{p(v)}{c q(v)}] \\ &= \frac{1}{\deg} \cdot \frac{p(v) \cdot \deg}{c} = \frac{p(v)}{c}, \end{aligned} \quad (6)$$

and the overall acceptance probability as:

$$\begin{aligned} \Pr[\text{accept}] &= \sum_{v \in N} \Pr[\text{sample} = v] \\ &= \frac{1}{c} \sum_{v \in N} p(v) = \frac{1}{c}. \end{aligned} \quad (7)$$

Thus, the conditional distribution of acceptance is:

$$\begin{aligned} \Pr[\text{sample} = v | \text{accept}] &= \frac{\Pr[\text{sample} = v]}{\Pr[\text{accept}]} \\ &= \frac{p(v)}{c} \div \frac{1}{c} = p(v) \end{aligned} \quad (8)$$

Hence, the probability distribution of the accepted node is the same as p , independent of the constant c . Therefore, using our insight to optimize RJS is not an approximate solution and does not harm the generality of sampling.

The remaining challenge is *how* to find a sufficient upper bound. Ideally, the estimate should satisfy two conditions. First, the bound must be close to the actual maximum weight; a bound far from this value enlarges the empty space in the 2D table and increases the expected number of trials before a successful sample. To achieve this, we estimate the maximum *per sampling step* rather than using a fixed value for all nodes, because the maximum depends heavily on node- and step-specific factors (e.g., the weight distribution of the current node and the degree of the previously visited node). Second, each estimation must be as lightweight as possible, since it will be performed repeatedly.

eRJS proposes to estimate the maximum value by following the variables and features used in the workload's edge weight computation function. Fig. 5a illustrates the baseline process of obtaining the boundary value using weighted Node2Vec. While the baseline can obtain the exact boundary value, it requires memory and weight computation per neighbor. Fig. 5b demonstrates how eRJS provides the estimated boundary with only a single memory access and three computations in the case of Node2Vec. We need to obtain the $\max(\hat{w}(v, u)) = \max(w(v, u) \cdot h(v, u))$, where we compute its upper bound as $\max(w(v, u)) \cdot \max(h(v, u))$. The former, $\max(w(v, u))$ is obtained from the walk algorithm (e.g., $\max(1/a, 1/b, 1)$), and the latter, $\max(h(v, u))$ can be

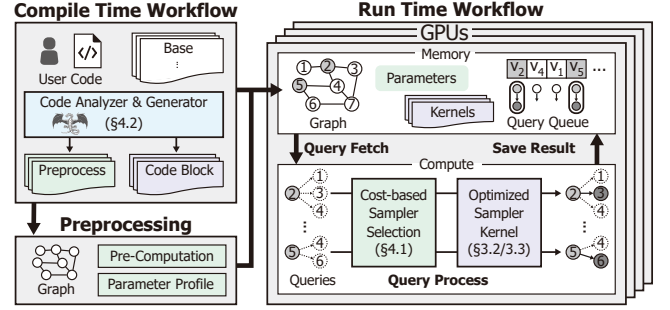


Figure 6. Overview of FLEXIWALKER framework.

preprocessed from the input graph dataset. By finding the max value of both variables, we can obtain the theoretically possible largest boundary per node.

We note that the aforementioned scheme has two potential pitfalls that hinder the general and efficient usage of eRJS. First, if the upper bound is still too far from the actual max weight, its overhead from the increased number of trials can outweigh the benefit of the eliminated max reduction. We avoid such cases by using a cost model to select the sampling strategy between rejection and reservoir during runtime, as explained in Section 4.1. Second, the estimation process highly depends on the individual random walk algorithm. This prohibits the use of a fixed estimation function for all workloads. One naive alternative would be to offload the implementation of the estimation function to the users. However, this would become a tedious process as users have to consider the constants/variables, whether to get the min/max value per variable, and also additional code to generate such values. We thus propose to automate the process of completing the max estimation pipeline with code analysis and generation in Section 4.2.

4 FLEXIWALKER Framework

FLEXIWALKER is a flexible framework that automatically runs the user-provided dynamic random walk logic with SOTA performance, using two optimized kernels in Section 3. To achieve this, the overall workflow consists of two components: compile-time and runtime workflow. Fig. 6 provides an overview of those components.

At compile time, FLEXI-COMPILER analyzes the user's workload implementation using LLVM/Clang [25] (Section 4.2). Specifically, FLEXI-COMPILER sweeps through the user code to detect the code structure and features that affect the neighbor sampling probability (e.g., max weight boundary). Based on the analysis, FLEXI-COMPILER generates human-readable parameters and code blocks, which are plugged into FLEXIWALKER's base framework code.

At runtime, FLEXIWALKER utilizes the code blocks and parameters from the compile-time workflow. Optionally, if some parameters (e.g., sampling cost per edge, max/sum of edge property weights) cannot be inferred statically since

they are runtime specific, FLEXIWALKER deploys a light-weight profiling and preprocessing phase to gather them. With these, FLEXI-RUNTIME concurrently fetches multiple walk queries from the query queue and relevant inputs to sample the next node for each query. For every walk step of each query, FLEXI-RUNTIME selects the most efficient sampling strategy using a generalizable cost model, informed by profiled data (parameters) and additional runtime-specific characteristics (Section 4.1). The selected strategy is executed via the eRJS and eRVS kernels (Section 3), which provide highly optimized kernels tailored to the dynamic nature of the workload.

4.1 FLEXI-RUNTIME

Performance Sensitivity to Weight Distribution. In Section 3.1, we observed that the best-performing sampling method depends on the environment. For a more in-depth analysis of the proposed optimized kernels, we compare the performance of eRVS and eRJS on weighted Node2Vec over the EU dataset in Fig. 7a. We artificially vary the skewness of the edge property weights h with a power-law distribution.

As shown in the results, eRVS shows consistent performance regardless of the distribution, as it always performs a single full scan over the entire transition weights. On the other hand, the performance of eRJS heavily depends on the skewness, because a single outlier can increase the maximum value, leading to many failed rejection sampling trials.

Additionally, we report the dynamic changes in transition weight distributions during runtime with 2nd PR in Fig. 7b. We aggregate the sum of edge weights for each node across multiple sampling steps. For these values, we calculate the coefficient of variation ($CV = std/mean \times 100$) for each node to quantify the relative variability of edge weights during runtime. The CVs across all nodes are then used to generate the histogram shown in the figure.

The x-axis indicates the upper bound of each histogram bin (i.e., CV range), and the y-axis denotes the number of nodes that fall into each bin. The CV metric enables fair comparison across nodes with different mean edge weights; higher CVs indicate greater fluctuations in edge weight sums across steps, highlighting nodes with more dynamic sampling behavior during runtime. As shown in the figure, a significant number of nodes exhibit high CV values (toward the right end of the histogram), highlighting substantial runtime variation. Together, the analysis suggests that selecting an appropriate kernel at runtime is crucial for optimal performance.

FLEXI-RUNTIME Design. Based on the above observation, we present FLEXI-RUNTIME, a runtime layer to choose the best-fitting sampling strategy for each step. To achieve the best performance, we opt to dynamically choose an adequate kernel for each individual step. For this purpose, we estimate the overhead of each sampling method by creating a lightweight first-order cost model.

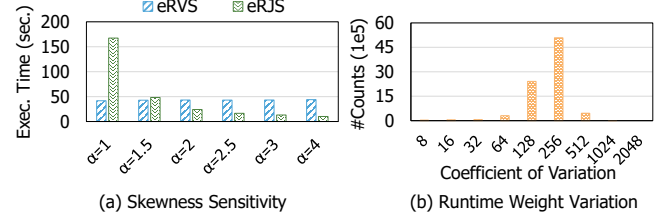


Figure 7. (a) Sensitivity study for reservoir and rejection sampling and (b) runtime weight variation with the EU dataset.

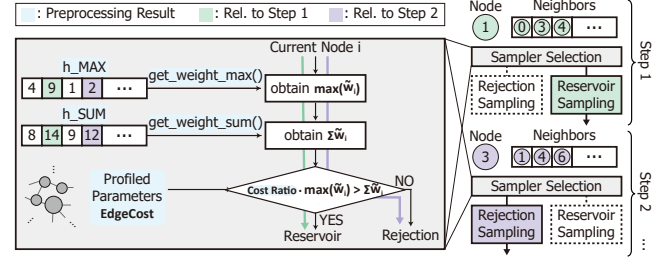


Figure 8. Overall procedure of FLEXI-RUNTIME.

Since both kernels are memory-dominated, our cost model takes into account the number of memory accesses in each method. From the procedures of eRJS and eRVS, we can develop a cost model for the number of edge weight accesses for the current target node. For eRVS, the memory cost is simply the degree of the current node v ,

$$Cost_{RVS} = EdgeCost_{RVS} \cdot degree, \quad (9)$$

where $EdgeCost_{RVS}$ is a sequential memory access cost per edge. For eRJS, the model is slightly complicated as we consider the expectation of the sampling trials.

$$Cost_{RJS} = EdgeCost_{RJS} \cdot degree \cdot \max_i(\tilde{w}_i) / \sum_i \tilde{w}_i. \quad (10)$$

In this equation, $EdgeCost_{RJS}$ is the random memory access cost per edge. The average number of accesses is estimated with the area of the 2D table ($degree \cdot \max_i(\tilde{w}_i)$) divided by the success space area ($\sum_i \tilde{w}_i$). Comparing the two yields the condition below for preferring eRJS over eRVS for the current node.

$$(EdgeCost_{RJS} / EdgeCost_{RVS}) \cdot \max_i(\tilde{w}_i) < \sum_i \tilde{w}_i. \quad (11)$$

The system parameter $EdgeCost_{RJS} / EdgeCost_{RVS}$ is profiled, as detailed in Section 5. Instead of $\max_i(\tilde{w}_i)$, we use its estimated upper bound due to the eRJS optimization. Similarly, we use an estimation of $\sum_i \tilde{w}_i$ because it dynamically changes, and exact computation is costly. From Eq. (1), and applying the linearity of expectation under the assumption that w and h are approximately independent, we estimate:

$$\sum_i \tilde{w}_i = \sum_i w_i h_i \approx \sum_i w_i \cdot E[h]. \quad (12)$$

Both values are obtained through compiler-assisted analysis, as described in Section 4.2.

4.2 FLEXI-COMPILER

We introduce FLEXI-COMPILER, a compile-time component for analyzing input functions and generating code blocks to provide an automated pipeline for optimizing dynamic random walk workloads. To realize this, FLEXI-COMPILER analyzes the given workload to determine which optimization techniques are applicable with the relevant parameters, specifically for rejection sampling. With the analysis results, FLEXI-COMPILER generates code building blocks that integrate into the end-to-end optimized framework. In the following, we explain the workflow of FLEXI-COMPILER.

We follow the popular gather-move-update programming model [48], where the core behavior is described in the `get_weight()` function as part of the gather phase. Specifically, for a random walk workload, FLEXI-COMPILER requires implementing the `init`, `get_weight`, `update` functions using the CUDA C++ API with the following contents:

- `init`: initializing workload-specific hyperparameters,
- `get_weight`: computing the current edge's weight,
- `update`: updating query-specific parameters after each walk step.

In particular, `get_weight()` receives the graph data, workload class, query-specific parameters, and an index of `get_weight()`'s target edge, and should return the target edge's weight. We present an example user code of weighted Node2Vec in Fig. 9a. Given fixed hyperparameters (a , b), the current neighbor being explored (`post`) and its edge property weight (h), weighted Node2Vec checks a number of conditions (green) to compute the final edge weight (purple).

With the input code, we deploy FLEXI-COMPILER's code analyzer, which consists of multiple components for code analysis. These include (i) Clang [25] LibTooling-based frontends for source-level abstract syntax tree (AST) analysis, and (ii) LLVM [25] IR-based backends for intermediate representation (IR) analysis. We integrate both components to enable the analysis of (potentially complex) input code (e.g., control flow checking, data-flow tracking, pointer chasing, alias analysis). Additionally, we illustrate how FLEXI-COMPILER views the given input code using a simplified syntax tree in Fig. 9b. Starting from the hyperparameters and initial `get_weight()` code snippets, each branch represents a possible control flow path, and leaves represent the corresponding return values.

We demonstrate how FLEXI-COMPILER's code analyzer operates in Fig. 9c, which comprises a dependency checker and a flag allocator. The dependency checker tracks expressions that both influence the return value and are necessary for the code generator to function properly. Examples include assignment statements or arithmetic operations of the variables that affect the return value. The flag allocator detects whether the upper bound estimation for eRJS is applicable to each return variable, and to the entire `get_weight()` function. Specifically, each flag represents the granularity

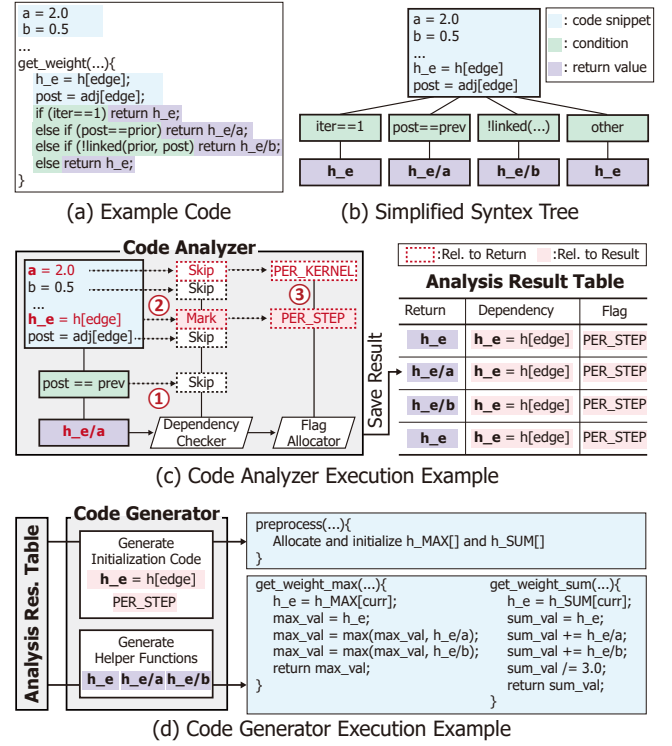


Figure 9. Overall procedure of FLEXI-COMPILER.

of weight upper bound estimations needed during runtime, which includes:

- PER_KERNEL: Only a single estimation is required (e.g., unweighted Node2Vec).
- PER_STEP: A boundary estimation per step is required (e.g., weighted Node2Vec).

For instance, if the return value uses indexed variables (e.g., h , the property weights), the flag allocator sets the flag to PER_STEP as the return value can change per step.

We demonstrate FLEXIWALKER processing an example return value `h_e/a` (Eq. (2)) as follows:

- ① The dependency checker traverses the syntax tree and encounters a condition/assignment expression for the `post` variable. These are skipped as they do not influence the return value.
- ② With additional tree traversal, the checker encounters relevant assignment statements for `h_e` and a . While we mark `h_e` to store it in the result table, a is skipped as it is a workload-specific fixed hyperparameter (i.e., the expression is not necessary for the code generation process).
- ③ In a similar manner, the flag allocator sets the flag for dependent values. Since `h_e` is assigned using an indexed value (h), the expression is flagged with PER_STEP.

The code analyzer repeats a similar process for each return branch. The results are then stored in an analysis result table, which is used in the next code generation step. It is worth mentioning that the code analyzer analyzes the code in a

fine-grained recursive manner in more detail: it recursively identifies all variables per relevant expression and launches different search processes for each variable (e.g., separate analysis processes for `h_e` and `a`).

As illustrated in Fig. 9d, FLEXI-COMPILER’s generator first outputs code snippets for preprocessing the identified relevant indexed values (`preprocess()`) with the analysis result table. The generated preprocessing code allocates and computes the max/sum of the relevant values using templates to create pointers (`h_MAX`). This is done by attaching predefined labels (`_MAX`) to the original indexed array (`h`). Next, code blocks are generated to call lightweight GPU reduction kernels for each new pointer.

Additionally, FLEXI-COMPILER’s generator outputs helper functions such as `get_weight_max()/_sum()` in Fig. 9d. These functions are called before each step to choose the sampling strategy in FLEXI-RUNTIME.

- The max helper function is generated by adding the dependent code snippets stored in the result table, and using dummy variables (e.g., `max_val`) to perform reduction operations for each return value.
- The sum helper function estimates the sum of weights with the average of all possible return values following Eq. (12). We start by replacing index variables with their new sum pointers (e.g., `h_SUM`). We accumulate all possible return values and divide them by the number of unique return values. For cases when `PER_KERNEL` is set, we multiply the final average by the degree to emulate the weight sum.

The resulting codes from the generator are integrated into FLEXIWALKER, completing the full deployable code base. We further discuss the generality of FLEXI-COMPILER by identifying scenarios where it cannot generate helper functions, and how such cases are addressed in Section 7.1.

5 Implementation

5.1 FLEXI-RUNTIME Profiling Kernels.

To improve the sampling method selection in FLEXI-RUNTIME, FLEXIWALKER deploys a lightweight profiling kernel to estimate the ratio of the overhead per edge weight computation. Before sampling, we run two kernels, where each kernel computes the weight value for a fixed ratio of the total nodes and a fixed number of their neighbors using eRJS and eRVS, respectively. By running the two lightweight kernels, the profiled ratio can indirectly incorporate hardware-specific features, such as cache hit and capacity. We design the kernel to only compute weights with a limited number of steps and queries, both of which minimize the profiling time as much as possible. Moreover, we also observed that limiting the number of computed edge weights allowed estimating the parameters in Eq. (11) with better performance, compared to simulating the sampling process for each query. We report the overhead of the profiling kernel in Section 6.5.

5.2 Concurrent Rejection and Reservoir Sampling.

FLEXI-RUNTIME maintains a random walk query for each thread, as rejection sampling requires only a single GPU thread for sampling. In contrast, reservoir sampling requires multiple coalesced memory accesses; it is more efficient to use at least 32 threads (i.e., CUDA warp). To address this gap in the optimal processing unit for each sampling method, we design a runtime kernel that works as follows:

1. Each thread within a warp fetches a query job and determines the sampling method with FLEXI-RUNTIME.
2. *RJS mode*: After a fixed number of independent rejection sampling trials, threads check whether a thread that requires reservoir sampling exists in the warp with CUDA warp intrinsics (e.g., `__ballot_sync()`).
 - a. *RVS mode*: If at least a single thread uses reservoir sampling, the warp synchronizes to share the target query hyperparameters (e.g., target node, step number) through additional warp intrinsics (e.g., `__shfl_sync()`). The entire warp then concurrently executes reservoir sampling.
 - b. If no thread uses reservoir sampling, we continue the process by returning to *RJS mode*.
3. We continue until all queries in the batch are processed.

Using this kernel design, we can switch between rejection and reservoir sampling with low overhead and deploy different thread granularities to each sampling method. Note that due to the implementation choice of switching between eRVS and eRJS, FLEXI-COMPILER returns warnings when inter-thread communication is detected in the user’s input code. Examples include warp intrinsics (e.g., `__ballot_sync()`) and synchronization functions (e.g., `__syncwarp()`).

5.3 Dynamic Query Scheduling.

FLEXIWALKER dynamically retrieves random walk queries from a global queue as individual processing units (i.e., GPU threads) complete their current query. We found that simply using a global counter representing the number of completed queries and an array of initial nodes was sufficient. Specifically, we use the global counter as an index to retrieve the initial node of the next target query from the array. The global counter is incremented atomically to avoid processing units accessing the same query.

6 Evaluation

6.1 Experimental Setup

To evaluate the performance of FLEXIWALKER, we conducted experiments on single- and multi-GPU computing environments with optimized software configurations. Our hardware setup consists of an AMD EPYC 9124P processor with 16 cores and 32 threads. The system is equipped with 512GB of DDR5 ECC memory. For GPU(s), we used up to four NVIDIA A6000 GPUs, each featuring 48GB of VRAM. On the software side, the experiments were conducted on Ubuntu 22.04.4 LTS.

Table 1. Real-World Graph Datasets.

Graph	#Vertices	#Edges
com-youtube (YT)	1.1M	6M
cit-patents (CP)	3.8M	33M
Livejournal (LJ)	4.8M	86M
Orkut (OK)	3.1M	234M
EU-2015 (EU)	11M	522M
Arabic-2005 (AB)	23M	1.1B
UK-2005 (UK)	39M	1.6B
Twitter (TW)	42M	2.4B
SK-2005 (SK)	51M	3.6B
Friendster (FS)	66M	3.6B

We utilized CUDA 12.1.1 (driver version 550.54.15) for GPU computations and cuRAND 10.3.2.106 for efficient random number generation.

We evaluate FLEXIWALKER using diverse real-world graph datasets from various domains, including social networks, citation networks, and web graphs. The detailed statistics of these datasets are presented in Table 1. These datasets vary significantly in size, ensuring a comprehensive evaluation across different scales. Datasets YT, CP, LJ, OK, and FS are obtained from Stanford SNAP [27], while EU, AB, UK, TW, and SK are from the Laboratory for Web Algorithmics (LAW) [3, 4]. This diverse dataset selection allows us to assess the scalability and effectiveness of FLEXIWALKER across various graph structures and domains. Following prior works [31, 48, 62], we generated random real numbers from $[1, 5)$ and random integers from $[0, 4]$ for datasets without edge property weights and edge labels, respectively.

We chose six baselines [17, 31, 37, 48, 53, 59], which are widely known CPU- or GPU-based random walk accelerations. Two baselines [48, 59] accelerate random walks using CPUs, while the other four baselines [17, 31, 37, 53] employ GPUs for random walk acceleration.

- SOWALKER [59]: state-of-the-art out-of-core CPU-based dynamic random walk framework utilizing RJS and ITS.
- THUNDERRW [48]: state-of-the-art CPU random walk framework supporting RJS (for unweighted Node2Vec) and ITS for dynamic random walks.
- C-SAW [37]: dynamic-extended version of ITS-based random walk GPU framework.
- NEXTDOOR [17]: RJS-based GPU random walk framework. It partially supports dynamic random walk (for unweighted Node2Vec).
- SKYWALKER [53]: dynamic-extended ALS-based GPU random walk framework.
- FLOWWALKER [31]: state-of-the-art GPU-based dynamic random walk framework with RVS.
- FLEXIWALKER (Proposed): our proposed framework.

If a baseline does not support a dynamic random walk workload, we faithfully extended it to support it by using the sampling methods employed in the baseline. For C-SAW, as it frequently faces out-of-memory issues and its original open-sourced implementation ignores high-degree nodes with

over 90,000 neighbors, we scaled the runtime according to the number of neighbors that it should have considered. Thus, the actual functionality of C-SAW is not exact when facing high-degree nodes, but we included the runtime results of C-SAW following the previous work [53].

We tested three famous dynamic random walk workloads, Node2Vec [12], MetaPath [8], and Second-Order PageRank (2nd PR) [58]. The method by which each workload obtains dynamic weights is described in Section 2.1. In the weighted version of a workload, the property weights h affect the transition weights, while the unweighted version uses only the workload-specific weights w to compute the transition weights. Unless specified otherwise, we use *weighted Node2Vec* as the main experiment target. Additionally, we report out-of-memory and out-of-time (i.e., execution time is longer than 12 hours) with *OOM* and *OOT*, respectively. We use the main random walk execution time for evaluation, and report FLEXIWALKER’s preprocessing/profiling time in Section 6.5. Following the prior GPU-based SOTA [31] on dynamic random walks, we set the number of walk steps to 80 for all workloads except MetaPath. For Node2Vec, we set $a = 2.0$ and $b = 0.5$. For MetaPath, we set the schema to $(0, 1, 2, 3, 4)$ and the depth to 5. For 2nd PR, we used $\gamma = 0.2$. We created walk queries for every node in the graph.

6.2 Performance Comparison

Uniform Property Weight Distribution. To benchmark the general dynamic random walk throughput of FLEXIWALKER compared with previous frameworks, we tested the uniform edge property weight distribution, which is widely adopted in the evaluation of previous approaches. Table 2 shows the execution time of FLEXIWALKER and baselines in such weight settings. We reported results from a total of five dynamic random walk workloads: (un)weighted Node2Vec, (un)weighted MetaPath, and 2nd PR.

FLEXIWALKER generally outperforms other baselines with kernel optimizations and dynamic runtime adaptation for intermediate weight distribution change. The speedups are significant, providing $4246.71\times$ maximum and $73.44\times$ geometric mean speedup over the best-performing cases of CPU baselines and $1040.54\times$ maximum and $5.91\times$ geometric mean speedup over the best-performing cases of GPU baselines. FLEXIWALKER achieves more speedup on weighted cases because weighted workloads typically suffer from excessive memory access to obtain max transition weights (i.e., NextDoor) or obtaining weight prefix sum (i.e., FlowWalker). For instance, in Node2Vec with AB, FLEXIWALKER shows much more speedup in the weighted cases than in the unweighted cases.

Many baselines with inverse transformation sampling and alias sampling often face out-of-time (OOT) on weighted Node2Vec and 2nd PR due to the significant overhead of their sampling methods. NEXTDOOR with rejection sampling also suffers from the same issue, since it requires heavy

Table 2. Execution time (ms) comparison with uniform property weight distribution on dynamic random walk workloads.

								OOM: out-of-memory		OOT: out-of-time (>12h)		
Method		YT	CP	LJ	OK	EU	AB	UK	FS	TW	SK	
Node2Vec	Unweighted	SOWALKER	2,099.58	6,753.56	10,929.20	8,068.65	29,798.90	61,960.30	151,586.00	2,978,360.00	1,339,820.00	542,455.00
		THUNDERRW	665.70	1,902.51	3,367.81	2,845.76	8,941.26	19,176.84	28,581.79	63,662.66	42,954.87	53,670.29
		C-SAW	28,310.38	4,913.03	35,323.08	39,010.11	1,288,951.02	4,046,140.56	OOT	457,827.27	OOT	OOT
		SKYWALKER	110,435.38	6,113.56	137,496.40	124,032.00	6,805,476.68	8,164,498.55	OOT	OOM	OOT	OOT
		FLOWWALKER	1,030.22	482.45	1,993.93	2,820.21	56,236.60	213,115.43	2,241,584.07	69,780.21	8,141,405.89	5,175,859.79
		NEXTDOOR	196.59	625.73	964.36	738.86	2,987.51	3,574.76	5,742.08	OOM	12,881.26	OOM
		FLEXIWALKER	127.18	477.91	522.80	373.74	1,354.21	1,725.79	3,086.15	7,974.53	6,310.56	4,974.23
	Weighted	SOWALKER	124,674.00	29,629.00	260,760.00	472,876.00	8,051,390.00	35,137,900.00	OOT	13,135,400.00	OOT	OOT
		THUNDERRW	33,579.50	20,023.04	152,158.13	330,548.73	3,320,409.43	8,062,093.25	OOT	14,678,644.89	OOT	OOT
		C-SAW	28,961.81	4,884.82	36,792.42	42,882.00	1,320,782.22	3,903,073.23	OOT	525,605.82	OOT	OOT
		SKYWALKER	5,583.29	1,963.64	13,975.75	19,956.82	371,165.81	1,177,678.10	OOT	OOM	OOT	OOT
		FLOWWALKER	1,114.12	520.10	2,143.03	3,036.36	62,627.75	234,367.61	2,454,958.59	75,460.18	8,943,632.52	5,659,740.15
		NEXTDOOR	8,062.29	2,552.00	32,963.51	76,708.57	1,028,338.67	5,774,621.92	OOT	OOM	OOT	OOM
		FLEXIWALKER	171.87	684.05	818.29	628.74	2,151.03	2,903.77	5,213.16	13,533.60	11,052.47	8,603.42
MetaPath	Unweighted	SOWALKER	265.93	1,116.85	1,643.64	2,422.68	5,573.99	13,692.90	26,722.80	108,808.00	51,601.00	71,366.80
		THUNDERRW	57.28	237.21	216.27	408.19	10,880.45	61,283.82	833,716.23	7,071.52	2,748,979.35	1,826,622.68
		C-SAW	234.45	252.11	1,363.60	2,536.96	36,345.29	141,196.29	3,057,522.79	14,040.36	7,948,156.03	3,631,413.87
		SKYWALKER	64.20	35.93	250.07	651.93	15,594.10	37,407.81	497,203.88	16,496.93	5,914,917.63	627,954.02
		FLOWWALKER	38.94	51.28	74.44	98.53	959.22	4,372.14	68,511.64	1,237.04	239,655.81	119,643.58
		NEXTDOOR	7.39	12.24	79.50	22.53	68.80	96.15	155.57	324.28	213.74	386.35
		FLEXIWALKER	4.57	17.27	20.20	20.52	44.16	88.01	151.21	320.25	210.56	227.91
	Weighted	SOWALKER	504.45	1,215.42	2,128.03	3,527.36	38,938.30	168,703.00	1,726,310.00	97,038.80	5,730,460.00	4,121,600.00
		THUNDERRW	89.30	253.47	336.72	1,158.42	15,849.39	83,312.79	1,056,136.86	11,299.45	1,422,630.00	2,352,756.81
		C-SAW	677.30	292.04	1,567.10	3,812.07	44,996.85	178,323.34	3,477,489.88	27,197.63	7,955,410.18	3,836,027.37
		SKYWALKER	75.96	42.09	302.60	786.33	13,864.43	63,707.60	832,796.04	20,815.26	7,673,433.84	4,297,459.35
		FLOWWALKER	39.33	53.23	83.20	135.59	1,367.38	8,594.29	142,880.65	1,710.89	493,637.27	260,334.52
		NEXTDOOR	11.90	14.87	29.64	60.02	201.63	541.65	4,371.89	927.33	13,789.51	10,418.03
		FLEXIWALKER	4.50	15.61	35.28	53.54	93.47	240.57	437.35	791.52	476.69	554.02
2nd PR	SOWALKER	753,675.00	104,357.00	898,852.00	1,464,480.00	OOT	OOT	OOT	35,616,800.00	OOT	OOT	
	THUNDERRW	35,234.79	18,467.97	150,269.48	330,437.24	3,583,335.52	9,079,893.14	OOT	14,337,824.58	OOT	OOT	
	C-SAW	36,200.17	11,657.34	47,228.58	55,622.71	1,689,041.36	4,760,768.13	OOT	528,260.39	OOT	OOT	
	SKYWALKER	6,081.96	2,227.76	10,754.80	16,314.03	358,016.67	1,266,910.14	OOT	OOM	OOT	OOT	
	FLOWWALKER	4,815.52	2,192.92	7,376.96	9,898.32	260,019.95	918,767.99	10,715,787.35	236,947.34	33,322,595.72	21,577,315.76	
	NEXTDOOR	7,965.82	2,234.03	33,063.51	76,072.33	1,143,994.88	6,451,071.85	OOT	OOM	OOT	OOM	
	FLEXIWALKER	455.44	412.54	634.65	490.10	23,923.95	28,552.45	291,228.69	10,440.54	1,596,040.01	896,175.64	

weight max reduction. On the other hand, FLEXIWALKER adopts lightweight and high-throughput eRJS and eRVS. As eRJS eliminates weight max reduce and eRVS minimizes the compute and memory access, FLEXIWALKER does not cause OOT in any cases and shows superior throughput in other baselines' OOT cases. In unweighted Node2Vec with SK, C-SAW and SKYWALKER suffer from OOT, but FLEXIWALKER does not, and provides 10.79 \times and 1040.54 \times speedup over the fastest CPU and GPU baselines, respectively.

FLEXIWALKER shows slight slowdowns on some cases with a relatively light workload (i.e., MetaPath). However, these cases are only confined to small datasets. For instance, in weighted MetaPath with CP, FLEXIWALKER faces 0.05% slowdown compared to NEXTDOOR, but this slowdown does not persist on the larger datasets (e.g., FLEXIWALKER provides 1.12 \times speedup over NEXTDOOR for OK). MetaPath has a relatively small number of sampling steps (in this case, five), and

hence, the running time is too short on small datasets. Due to the extremely short running time, the slight overhead of FLEXIWALKER causes some slowdowns.

Power-Law Property Weight Distribution. To further test the flexibility of FLEXIWALKER on various types of weight distributions, we initialized the edge property weight distribution of graphs to a power-law distribution and benchmarked the dynamic random walk throughput of FLEXIWALKER and baselines. For the initialization, we utilized `np.random.pareto` function in numpy library. To emulate the various power-law distributions, we used the Pareto distribution shape value (α) from 1.0 to 4.0. Fig. 10 shows the dynamic random walk execution time of NEXTDOOR, FLOWWALKER, and FLEXIWALKER for graphs with power-law weight distribution. We plotted the bars with a log scale, since NEXTDOOR takes too much time compared to FLEXIWALKER. We included the results of NEXTDOOR and FLOWWALKER

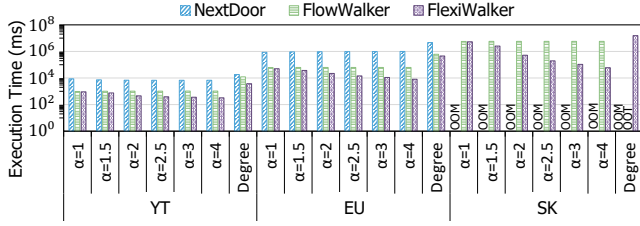


Figure 10. Performance comparison with power-law and degree-based edge property weight distribution.

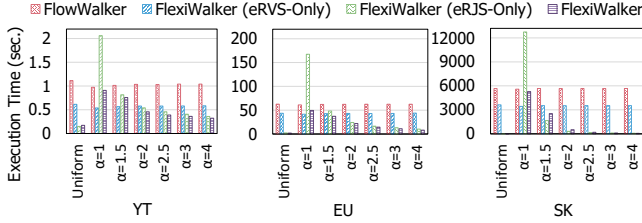


Figure 11. Performance of FLEXIWALKER's runtime component with uniform and power-law weight distribution. Other than FLOWWALKER, all three results are from FLEXIWALKER.

as they are representative GPU-based rejection sampling and reservoir sampling accelerations and typically showed the highest throughput compared to other baselines in Table 2. Overall, FLEXIWALKER provides 26.60 \times , 4.37 \times geometric mean speedup over NEXTDOOR and FLOWWALKER, respectively. FLEXIWALKER is more robust on skewed distributions (with lower α), thereby showing stable execution time when α is changed. NEXTDOOR suffers from the GPU out-of-memory (OOM) issue in the largest SK dataset because it internally uses sorting to exploit memory locality, and thus this sorting requires additional memory usage compared to FLEXIWALKER and FLOWWALKER.

Degree-Based Property Weight Distribution. Lastly, we tested FLEXIWALKER and baselines with edge property weights generated with the neighboring node's degree in Fig. 10. Due to the nodes with larger degrees having larger edge weights, we observed all baselines taking longer compared to the execution time with uniform and power-law weight distributions. Nevertheless, FLEXIWALKER outperformed NEXTDOOR and FLOWWALKER up to 10.24 \times and 3.29 \times speedup, respectively. Moreover, FLEXIWALKER was able to compute all queries in the SK dataset, while both baselines failed either due to OOM or out-of-time (OOT) issues.

6.3 Ablation Studies

We conducted ablation studies to verify the effect of FLEXIWALKER's runtime component, which adaptively selects the sampling kernel and kernel optimizations.

Runtime Component. To check the advantage of the runtime component of FLEXIWALKER, we compared FLEXIWALKER's runtime component with eRJS-only and eRVS-only

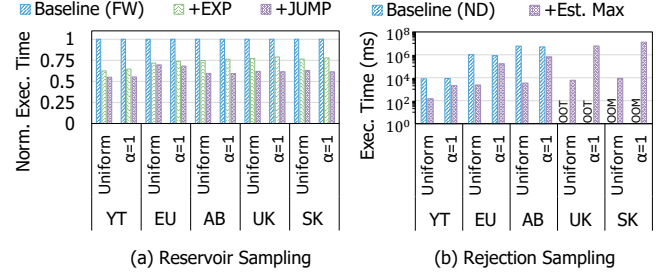


Figure 12. Ablation study of optimization techniques for (a) reservoir sampling and (b) rejection sampling kernels for uniform and skewed ($\alpha = 1$) weight distributions.

versions of FLEXIWALKER in Fig. 11. Such single-method versions do not change the sampling kernel during the entire walk procedure. We additionally included FLOWWALKER as a reference, as it is the fastest baseline in weighted Node2Vec. We tested both graphs with uniform weight distribution (leftmost) and power-law weight distribution (right). We can observe that eRVS shows stable performance across varying weight skews, while eRJS's performance degrades as the weight distribution becomes more skewed. Moreover, for both weight distributions, since the eRJS and eRVS of FLEXIWALKER fail to adapt to node characteristics, FLEXIWALKER with the runtime sampling method selection provides up to 3.37 \times and 421.56 \times speedup over the eRJS and eRVS versions, respectively. Note that there are cases where eRVS/eRJS outperforms the runtime component (e.g., $\alpha = 1$ and $\alpha = 1.5$ in SK). This is due to the runtime component selecting the less optimal sampling strategy for certain instances. Nevertheless, the runtime component can prevent slowdown when using only either eRJS or eRVS (e.g., in highly skewed distributions ($\alpha = 1$), eRJS is significantly slower than eRVS). Overall, this shows the importance of capturing node-specific features during execution in dynamic random walks with the runtime component in FLEXIWALKER.

Kernel Optimizations. We further micro-benchmarked the sole effect of kernel optimizations, eRJS and eRVS, in Fig. 12 with uniform and skewed weight distributions ($\alpha = 1$). In Fig. 12a, we compared eRVS with the SOTA reservoir sampling (i.e., FLOWWALKER). eRVS's advantages compared to FLOWWALKER are twofold: reduced memory access (EXP) and computation (JUMP). With only the former, it provides 1.30-1.60 \times and 1.27-1.55 \times speedup over FLOWWALKER, and by adding the latter, FLEXIWALKER provides 1.44-1.82 \times and 1.47-1.81 \times speedup over FLOWWALKER with uniform and skewed weight distribution, respectively. In Fig. 12b, we tested eRJS compared to state-of-the-art rejection sampling, NEXTDOOR. As eRJS bypasses redundant max reductions with bound estimation, it significantly outperforms NEXTDOOR from 54.49 \times to 1698.35 \times in uniform weight distribution. Similarly, with skewed weight distributions, eRJS outperforms NEXTDOOR by up to 7.27 \times . We believe the relatively lower speedup

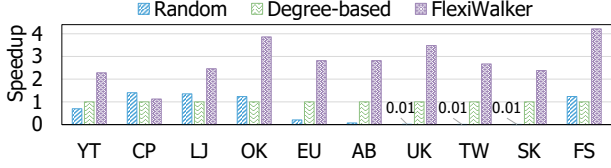


Figure 13. Sensitivity study on sampling method selection strategy (random, degree-based, and FLEXIWALKER’s cost model).

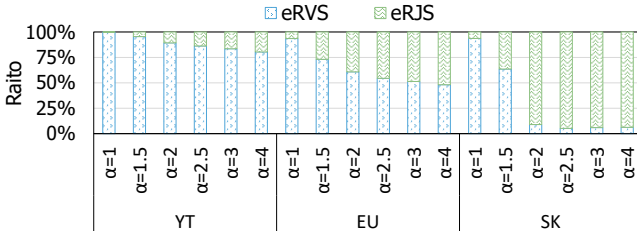


Figure 14. The ratio of chosen sampling method in various power-law weight distributions.

stems from the skewed distribution, where a large number of candidates are rejected during the sampling process.

6.4 Analyses of Sampling Algorithm Selection Strategy

Sensitivity on Selection Strategy. To verify whether the sampling algorithm selection engine of FLEXIWALKER is adequate, we compared FLEXIWALKER with the other two selection strategies, random and degree-based selection in Fig. 13. We report the speedup normalized against degree-based selection. Random selection randomly picks the sampling algorithm between rejection and reservoir sampling. Degree-based selection employs reservoir sampling when the degree of a node is less than 1K and adopts rejection sampling otherwise, since rejection sampling is more robust for processing high-degree nodes. FLEXIWALKER achieves speedup over random selection and degree-based selection, providing 15.86× and 2.66× geometric mean speedup over them.

Ratio of Selected Algorithms. As FLEXIWALKER adaptively selects the sampling algorithm during the walk procedure, it is worth profiling the actual ratio of selection between the two base algorithms, rejection and reservoir samplings. In Fig. 14, we profiled the ratio of the chosen sampling method with YT, EU, and SK. To extract further insight, we tested various power-law Pareto distribution shape values (α) ranging from 1.0 to 4.0 (lower values indicate a more skewed distribution). Since rejection sampling is less robust to skewed distributions than reservoir sampling, rejection sampling is far less selected in skewed distributions with lower α . This shows that FLEXIWALKER adequately selects the proper sampling algorithms based on the edge probability distribution.

Table 3. Profile and Preprocessing Time (ms).

Time (ms)	YT	CP	LJ	OK	EU	AB	UK	FS	TW	SK
Profile	6.31	6.78	7.68	7.13	11.03	16.72	27.76	12.13	9.76	10.70
Preproc.	0.54	1.65	2.31	2.62	7.77	17.11	25.08	58.40	40.70	67.34
Total	6.85	8.43	9.99	9.75	18.80	33.83	52.84	70.53	50.46	78.04

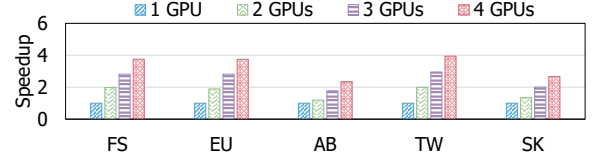


Figure 15. Multi-GPU scalability.

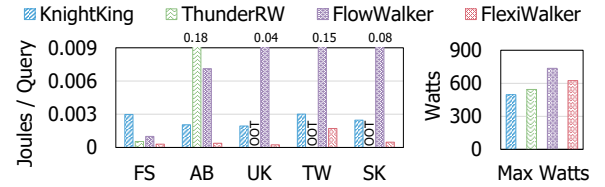


Figure 16. Energy efficiency comparison.

6.5 Analysis on Overheads

To verify that FLEXIWALKER incurs small additional overhead compared to workload running time, we show the profiling and preprocessing time of FLEXIWALKER on all datasets in Table 3. Compared to the execution time of weighted Node2Vec, the profiling and preprocessing time are extremely small, requiring only 0.46%-3.98% of the total running time. Also, it is worth noting that those profiled and preprocessed results are reusable per workload and/or graph.

6.6 Multi-GPU Scalability

We also benchmarked whether FLEXIWALKER is scalable with multiple GPUs. Fig. 15 illustrates the scalability of FLEXIWALKER as the number of GPUs increases from one to four. We distributed the queries into GPUs with hash-based index mapping of the starting nodes because naïve range-based index mapping showed lower scalability. The input graph was duplicated on all GPUs. Since this query parallelism is highly efficient, FLEXIWALKER achieves stable scalability with multiple GPUs, showing 3.23× geometric mean speedup over the single GPU case using four GPUs. In AB, FLEXIWALKER scales less efficiently due to the remaining workload imbalance among GPUs, but still provides 2.35× speedup over the single GPU case when utilizing four GPUs.

6.7 Energy Efficiency

Lastly, we compared the energy efficiency of FLEXIWALKER against CPU and GPU baselines. In addition to THUNDERRW (CPU) and FLOWWALKER (GPU), we included another established CPU baseline, KNIGHTKING [62]. We report both the

energy efficiency in joules per query and the maximum reported watts of each baseline across all datasets in Fig. 16. We observed KNIGHTKING requiring less energy compared to both THUNDERRW and FLOWWALKER, except for FS. However, FLEXIWALKER was able to achieve the highest energy efficiency with up to $10.15\times$ less joules per query compared to KNIGHTKING. Moreover, while FLEXIWALKER required higher max watts compared to the CPU baselines, it used $1.18\times$ less maximum power (watts) than FLOWWALKER (GPU).

7 Discussion

7.1 Limitations

We discuss the limitations of FLEXIWALKER, focusing on two scenarios where FLEXI-COMPILER is unable to derive an appropriate upper bound for eRJS. One scenario is when graph topology-related values are updated during runtime (e.g., updates on edge property weights in dynamic graphs). Such updates can compromise the accuracy of preprocessed values (e.g., maximum edge property weight), thereby impacting the functionality of eRJS. Another case stems from complex user input code, where FLEXI-COMPILER can generate incorrect code for `get_weight_max()/sum()`. FLEXI-COMPILER thus checks the user code for convoluted loops such as recursive function calls, loops with data-dependent exits, and deeply nested structures. When FLEXI-COMPILER detects such scenarios, it focuses on soundness by safely falling back to eRVS-only mode. Nevertheless, FLEXIWALKER was able to generate code for all five random walk workloads and utilize eRJS in Section 6. We believe FLEXIWALKER will be applicable to most dynamic random walk workloads.

7.2 Future Extensions

Despite already providing a flexible GPU framework for various dynamic random walk applications, FLEXIWALKER has the potential to support additional scenarios. First, we can target larger graphs by allocating graph partitions to different GPUs, similar to distributed GNN frameworks [38, 47]. While possible with graph partitioners [19] and inter-GPU communication libraries [33, 34], we expect considerable communication overhead due to the I/O-bound nature of random walks. Second, FLEXIWALKER can be extended to support dynamic graphs with modules that update the preprocessed values and graph topology. FLEXIWALKER's design could potentially provide performance benefits for dynamic graphs, especially FLEXI-RUNTIME, since it can choose different sampling methods per sampling step. Finally, FLEXIWALKER can support low-precision edge weights to reduce memory bandwidth usage. To demonstrate, we compared the performance of FLEXIWALKER against FLOWWALKER with weighted Node2Vec using INT8 to store edge property weights (generated with uniform weight distribution). FLEXIWALKER still outperformed FLOWWALKER by $27.59\times$ geometric mean speedup, demonstrating the applicability of FLEXIWALKER.

8 Related Work

8.1 CPU-Based Acceleration of Random Walks

Extending static and dynamic random walks to large graphs [1, 22, 24] can be challenging, primarily due to the sheer volume of data and the inherent workload imbalance. To address such issues, various works target CPUs to optimize random walks [18, 23, 28, 32, 43, 55, 56, 59, 62]. DrunkardMob and GraphWalker extend GraphChi for out-of-core simulation [23, 24, 55]. KnightKing distributes walks with load balancing, using alias sampling for static and rejection sampling for dynamic cases [62]. A memory-aware framework [43] analytically selects between different sampling methods but approximates transition weights. NosWalker decouples disk I/O from computation for higher throughput [56], while GraSorw and SOWalker further optimize out-of-core processing [28, 59]. Nonetheless, most schemes still favor static walks or remain bounded by CPU resources.

8.2 GPU-Based Acceleration of Random Walks

Several works [17, 31, 37, 53, 54, 60] have accelerated random walks using GPUs. C-SAW [37] utilizes the inverse transform sampling algorithm with warp-centric parallelism. NextDoor [17] performs graph sampling based on rejection sampling by gathering workloads with the same target using transit parallelism. SkyWalker [53, 54] and CoWalker [60] employ alias sampling on GPUs. FlowWalker [31] is the current state-of-the-art GPU framework for dynamic random walks. The aforementioned solutions either target static random walks or are burdened by additional performance bottlenecks arising from dynamic random walk traits. FLEXIWALKER efficiently alleviates such issues using efficient kernels and generalizable optimization techniques.

9 Conclusion

We propose FLEXIWALKER, an extensible framework for dynamic random walks. FLEXIWALKER proposes efficient rejection and reservoir sampling kernels, a lightweight cost model for runtime sampling method selection, and compile-time automatic workload optimization and specialization. FLEXIWALKER achieves $73.44\times$ and $5.91\times$ geometric mean speedup over CPU and GPU baselines' best performing cases, respectively.

Acknowledgments

This work was partially supported by Institute of Information & communications Technology Planning & Evaluation (IITP) (RS-2024-00395134, RS-2024-00347394, RS-2023-00256081, RS-2021II211343). Part of the infrastructure used in this work was supported by Korea Basic Science Institute (National research Facilities and Equipment Center) grant funded by the Ministry of Science and ICT (No. RS-2025-00564840). Jinho Lee is the corresponding author.

References

- [1] Lars Backstrom, Dan Huttenlocher, Jon Kleinberg, and Xiangyang Lan. 2006. Group Formation in Large Social Networks: Membership, Growth, and Evolution. In *KDD*. ACM, Philadelphia, PA, USA, 44–54.
- [2] Ayan Kumar Bhowmick, Koushik Meneni, Maximilien Danisch, Jean-Loup Guillaume, and Bivas Mitra. 2020. Louvainne: Hierarchical louvain method for high quality and scalable network embedding. In *WSDM*. ACM, Houston, TX, USA, 43–51.
- [3] Paolo Boldi, Marco Rosa, Massimo Santini, and Sebastiano Vigna. 2011. Layered Label Propagation: A MultiResolution Coordinate-Free Ordering for Compressing Social Networks. In *WWW*. ACM, Hyderabad, India, 587–596.
- [4] Paolo Boldi and Sebastiano Vigna. 2004. The WebGraph Framework I: Compression Techniques. In *WWW*. ACM, New York, NY, USA, 595–602.
- [5] Sudhanshu Chappuriya and Cameron Musco. 2020. Infinitewalk: Deep network embeddings as laplacian embeddings with a nonlinearity. In *KDD*. ACM, Virtual Event, CA, USA, 1325–1333.
- [6] Burgess Davis. 1990. Reinforced random walk. *Probability Theory and Related Fields* 84, 2 (1990), 203–229.
- [7] Luc Devroye. 1986. *Nonuniform random variate generation*. Springer, New York, NY, USA.
- [8] Yuxiao Dong, Nitesh V. Chawla, and Ananthram Swami. 2017. meta-path2vec: Scalable Representation Learning for Heterogeneous Networks. In *KDD*. ACM, Halifax, NS, Canada, 135–144.
- [9] Pavlos S Efthymiou and Paul G Spirakis. 2006. Weighted random sampling with a reservoir. *Inform. Process. Lett.* 97, 5 (2006), 181–185.
- [10] Dániel Fogaras and Balázs Rácz. 2004. Towards scaling fully personalized pagerank. In *WAW*. Springer, Rome, Italy, 105–117.
- [11] Joseph E. Gonzalez, Yucheng Low, Haijie Gu, Danny Bickson, and Carlos Guestrin. 2012. PowerGraph: Distributed Graph-Parallel Computation on Natural Graphs. In *OSDI*. USENIX, Hollywood, CA, USA, 17–30.
- [12] Aditya Grover and Jure Leskovec. 2016. node2vec: Scalable Feature Learning for Networks. In *KDD*. ACM, San Francisco, California, USA, 855–864.
- [13] Farzaneh Heidari and Manos Papagelis. 2020. Evolving network representation learning based on random walks. *Applied network science* 5, 1 (2020), 1–38.
- [14] Shixun Huang, Zhifeng Bao, Guoliang Li, Yanghao Zhou, and J Shane Culpepper. 2020. Temporal network representation learning via historical neighborhoods aggregation. In *ICDE*. IEEE, Dallas, TX, USA, 1117–1128.
- [15] Zexi Huang, Arlei Silva, and Ambuj Singh. 2021. A broader picture of random-walk based graph embedding. In *KDD*. ACM, Virtual Event, Singapore, 685–695.
- [16] Lorenz Hübschle-Schneider and Peter Sanders. 2022. Parallel weighted random sampling. *ACM TOMS* 48, 3 (2022), 40 pages.
- [17] Abhinav Jangda, Sandeep Polisetty, Arjun Guha, and Marco Serafini. 2021. Accelerating graph sampling for graph machine learning using GPUs. In *EuroSys*. ACM, Online Event, United Kingdom, 311–326.
- [18] Jinhong Jung, Namyoung Park, Sael Lee, and U Kang. 2017. BePI: Fast and Memory-Efficient Method for Billion-Scale Random Walk with Restart. In *SIGMOD*. ACM, Chicago, Illinois, USA, 789–804.
- [19] George Karypis and Vipin Kumar. 1998. A fast and high quality multilevel scheme for partitioning irregular graphs. *SIAM Journal on scientific Computing* 20, 1 (1998), 359–392.
- [20] Farzad Khorasani, Keval Vora, Rajiv Gupta, and Laxmi N. Bhuyan. 2014. CuSha: Vertex-Centric Graph Processing on GPUs. In *HPDC*. ACM, Vancouver, BC, Canada, 239–252.
- [21] Shima Khoshraftar, Sedigheh Mahdavi, Aijun An, Yonggang Hu, and Junfeng Liu. 2019. Dynamic graph embedding via lstm history tracking. In *DSAA*. IEEE, Washington, D.C., USA, 119–127.
- [22] Haewoon Kwak, Changhyun Lee, Hosung Park, and Sue Moon. 2010. What is Twitter, a social network or a news media?. In *WWW*. ACM, Raleigh, NC, USA, 591–600.
- [23] Aapo Kyrola. 2013. DrunkardMob: Billions of Random Walks on Just a PC. In *RecSys*. ACM, Hong Kong, China, 257–264.
- [24] Aapo Kyrola, Guy Blelloch, and Carlos Guestrin. 2012. GraphChi: Large-Scale Graph Computation on Just a PC. In *OSDI*. USENIX, Hollywood, CA, USA, 31–46.
- [25] Chris Lattner and Vikram Adve. 2004. LLVM: A compilation framework for lifelong program analysis & transformation. In *CGO*. IEEE, San Jose, CA, USA, 75–86.
- [26] Jinho Lee, Heesu Kim, Sungjoo Yoo, Kiyoung Choi, H. Peter Hofstee, Gi-Joon Nam, Mark R. Nutter, and Damir Jamsek. 2017. ExtraV: Boosting Graph Processing Near Storage with a Coherent Accelerator. *pVLDB* 10, 12 (2017), 1706–1717.
- [27] Jure Leskovec and Andrej Krevl. 2014. SNAP Datasets: Stanford large network dataset collection. <https://snap.stanford.edu/>
- [28] Hongzheng Li, Yingxia Shao, Junping Du, Bin Cui, and Lei Chen. 2022. An I/O-Efficient Disk-based Graph System for Scalable Second-Order Random Walk of Large Graphs. *pVLDB* 15, 8 (2022), 1619–1631.
- [29] Steffen Maass, Changwoo Min, Sanidhya Kashyap, Woonhak Kang, Mohan Kumar, and Taesoo Kim. 2017. Mosaic: Processing a Trillion-Edge Graph on a Single Machine. In *EuroSys*. ACM, Belgrade, Serbia, 527–543.
- [30] Grzegorz Malewicz, Matthew H. Austern, Aart J.C Bik, James C. Dehnert, Ilan Horn, Naty Leiser, and Grzegorz Czajkowski. 2010. Pregel: A System for Large-scale Graph Processing. In *SIGMOD*. ACM, Indianapolis, IN, USA, 135–146.
- [31] Junyi Mei, Shixuan Sun, Chao Li, Cheng Xu, Cheng Chen, Yibo Liu, Jing Wang, Cheng Zhao, Xiaofeng Hou, Minyi Guo, et al. 2024. FlowWalker: A Memory-Efficient and High-Performance GPU-Based Dynamic Graph Random Walk Framework. *pVLDB* 17, 8 (2024), 1788–1801.
- [32] Songjie Niu and Dongyan Zhou. 2021. SOOP: Efficient Distributed Graph Computation Supporting Second-Order Random Walks. *JCSST* 36, 5 (2021), 985–1001.
- [33] NVIDIA. 2025. NCCL. <https://github.com/NVIDIA/nccl>, visited on 2025-09-01.
- [34] NVIDIA. 2025. NVSHMEM. <https://developer.nvidia.com/nvshmem>, visited on 2025-09-01.
- [35] Sheehan Olver and Alex Townsend. 2013. Fast inverse transform sampling in one and two dimensions. *arXiv:1307.1223*
- [36] Lawrence Page, Sergey Brin, Rajeev Motwani, and Terry Winograd. 1999. *The PageRank Citation Ranking: Bringing Order to the Web*. Technical Report. Stanford infolab.
- [37] Santosh Pandey, Lingda Li, Adolfo Hoisie, Xiaoye S. Li, and Hang Liu. 2020. C-SAW: A Framework for Graph Sampling and Random Walk on GPUs. In *SC*. IEEE, Virtual Event, 1–15.
- [38] Jingshu Peng, Zhao Chen, Yingxia Shao, Yanyan Shen, Lei Chen, and Jiannong Cao. 2022. Sancus: Staleness-Aware Communication-Avoiding Full-Graph Decentralized Training in Large-Scale Graph Neural Networks. *pVLDB* 15, 9 (2022), 1937–1950.
- [39] Bryan Perozzi, Rami Al-Rfou, and Steven Skiena. 2014. DeepWalk: online learning of social representations. In *KDD*. ACM, New York, NY, USA, 701–710.
- [40] Leonardo FR Ribeiro, Pedro HP Saverese, and Daniel R Figueiredo. 2017. struc2vec: Learning node representations from structural identity. In *KDD*. ACM, Halifax, NS, Canada, 385–394.
- [41] Christian P Robert, George Casella, and George Casella. 1999. *Monte Carlo statistical methods*. Vol. 2. Springer, New York, NY, USA.
- [42] S. Khoshraftar S. Mahdavi and A. An. 2018. dynnode2vec: Scalable Dynamic Network Embedding. In *BigData*. IEEE, Seattle, WA, USA, 3762–3765.
- [43] Yingxia Shao, Shiyue Huang, Xupeng Miao, Bin Cui, and Lei Chen. 2020. Memory-Aware Framework for Efficient Second-Order Random Walk on Large Graphs. In *SIGMOD*. ACM, Portland, OR, USA, 1797–1812.

- [44] Changmin Shin, Taehee Kwon, Jaeyong Song, Jae Hyung Ju, Frank Liu, Yeonkyu Choi, and Jinho Lee. 2024. A Case for In-Memory Random Scatter-Gather for Fast Graph Processing. *IEEE CAL* 23, 1 (2024), 73–77.
- [45] Changmin Shin, Jaeyong Song, Hongsun Jang, Dogeun Kim, Jun Sung, Taehee Kwon, Jae Hyung Ju, Frank Liu, Yeonkyu Choi, and Jinho Lee. 2025. Piccolo: Large-Scale Graph Processing with Fine-Grained In-Memory Scatter-Gather. In *HPCA*. IEEE, Las Vegas, NV, USA, 641–656.
- [46] Julian Shun and Guy E. Blelloch. 2013. Ligra: A Lightweight Graph Processing Framework for Shared Memory. In *PPoPP*. ACM, Shenzhen, China, 135–146.
- [47] Jaeyong Song, Hongsun Jang, Hunseong Lim, Jaewon Jung, Youngsok Kim, and Jinho Lee. 2024. GraNNDis: Fast Distributed Graph Neural Network Training Framework for Multi-Server Clusters. In *PACT*. ACM, Long Beach, CA, USA, 91–107.
- [48] Shixuan Sun, Yuhang Chen, Shengliang Lu, Bingsheng He, and Yuchen Li. 2021. ThunderRW: an in-memory graph random walk engine. *pVLDB* 14, 11 (2021), 1992–2005.
- [49] Jeffrey S. Vitter. 1985. Random Sampling with a Reservoir. *ACM TOMS* 11, 1 (1985), 37–57.
- [50] John Von Neumann. 1951. Various techniques used in connection with random digits. *Applied Math Series* 12, 36–38 (1951), 3.
- [51] Alastair J. Walker. 1977. An Efficient Method for Generating Discrete Random Variables with General Distributions. *ACM TOMS* 3, 3 (1977), 253–256.
- [52] Hao Wang, Enhong Chen, Qi Liu, Tong Xu, Dongfang Du, Wen Su, and Xiaopeng Zhang. 2018. A united approach to learning sparse attributed network embedding. In *ICDM*. IEEE, Singapore, Singapore, 557–566.
- [53] Pengyu Wang, Chao Li, Jing Wang, Taolei Wang, Lu Zhang, Jingwen Leng, Quan Chen, and Minyi Guo. 2021. Skywalker: Efficient Alias-Method-Based Graph Sampling and Random Walk on GPUs. In *PACT*. IEEE, Atlanta, GA, USA, 304–317.
- [54] Pengyu Wang, Cheng Xu, Chao Li, Jing Wang, Taolei Wang, Lu Zhang, Xiaofeng Hou, and Minyi Guo. 2023. Optimizing GPU-Based Graph Sampling and Random Walk for Efficiency and Scalability. *IEEE TC* 72, 9 (2023), 2508–2521.
- [55] Rui Wang, Yongkun Li, Hong Xie, Yinlong Xu, and John C. S. Lui. 2020. GraphWalker: An I/O-Efficient and Resource-Friendly Graph Analytic System for Fast and Scalable Random Walks. In *ATC*. USENIX, Virtual Event, 559–571.
- [56] Shuke Wang, Mingxing Zhang, Ke Yang, Kang Chen, Shaonan Ma, Jinlei Jiang, and Yongwei Wu. 2023. NosWalker: A Decoupled Architecture for Out-of-Core Random Walk Processing. In *ASPLOS*. ACM, Vancouver, BC, Canada, 466–482.
- [57] Yangzihao Wang, Andrew Davidson, Yuechao Pan, Yuduo Wu, Andy Riffel, and John D. Owens. 2016. Gunrock: A High-Performance Graph Processing Library on the GPU. In *PPoPP*. ACM, Barcelona, Spain, 1–12.
- [58] Yubao Wu, Yuchen Bian, and Xiang Zhang. 2016. Remember where you came from: on the second-order random walk based proximity measures. *pVLDB* 10, 1 (2016), 13–24.
- [59] Yutong Wu, Zhan Shi, Shicai Huang, Zhipeng Tian, Pengwei Zuo, Peng Fang, and Dan Feng. 2023. SOWalker: An I/O-Optimized Out-of-Core Graph Processing System for Second-Order Random Walks. In *ATC*. USENIX, Boston, MA, USA, 87–100.
- [60] Cheng Xu, Chao Li, Pengyu Wang, Xiaofeng Hou, Jing Wang, Shixuan Sun, Minyi Guo, Hanqing Wu, Dongbai Chen, and Xiangwen Liu. 2023. High-Throughput GPU Random Walk with Fine-Tuned Concurrent Query Processing. In *PPoPP*. ACM, Montreal, QC, Canada, 432–434.
- [61] Ke Yang, Xiaosong Ma, Saravanan Thirumuruganathan, Kang Chen, and Yongwei Wu. 2021. Random walks on huge graphs at cache efficiency. In *SOSP*. ACM, Virtual Event, Germany, 311–326.
- [62] Ke Yang, MingXing Zhang, Kang Chen, Xiaosong Ma, Yang Bai, and Yong Jiang. 2019. KnightKing: a fast distributed graph random walk engine. In *SOSP*. ACM, Huntsville, ON, Canada, 524–537.
- [63] Chuxu Zhang, Dongjin Song, Chao Huang, Ananthram Swami, and Nitesh V Chawla. 2019. Heterogeneous graph neural network. In *KDD*. ACM, Anchorage, AK, USA, 793–803.
- [64] Chang Zhou, Yuqiong Liu, Xiaofei Liu, Zhongyi Liu, and Jun Gao. 2017. Scalable graph embedding for asymmetric proximity. In *AAAI*. AAAI, San Francisco, California, USA, 2942–2948.